Cross-spectral analysis of the B-star drag term and solar and geomagnetic activity indices

Volodymyr Komendant[1], Artem Sukharev[2,3]
[1] Space Research and Technology Institute, Bulgarian Academy of Sciences, Sofia
[2] Institute of Radio Astronomy NAS of Ukraine, Kharkiv
[3] Ventspils University of Applied Sciences, Latvia
vova_komendant@space.bas.bg; votan1360@gmail.com
(Submitted on 21.04.2026; Accepted on 18.06.2026)

Abstract. Cross-spectral analysis of time series is a technique in spectral analysis that is used to study the relationship between two time series in the frequency domain. It is especially useful when one is interested not just in whether there is a relationship, but also in the frequencies at which that relationship is expressed. Regression models were used to obtain the set of indices that have the greatest influence on the drag parameter of the studied satellite. Then these indices were used in cross-spectral analysis. For a joint analysis, the drag coefficient was taken for three satellites moving at mid-latitudes. Interrelated periods for the satellite drag coefficient and the selected indices of solar and geomagnetic activity were obtained. The strength and linearity of the obtained interrelations are shown graphically, along with the phase shifts between the interrelated periods.
Key words: B-star drag term, solar activity, space weather

Introduction

Before the space age, the Earth's atmosphere was studied using observations of meteoroids burning in it, radar, airglow, rockets, and weather balloons. All of these methods were limited in altitude (usually working up to an altitude of 150 km). After the launch of the first artificial Earth satellite (Sputnik-1), humanity gained the opportunity to study the atmosphere directly with the help of instruments aboard spacecraft. Not only was the atmosphere's density measured, but its composition was also measured at different altitudes. Thus, scientists obtained a set of data that helped expand our knowledge about the atmosphere of our planet [Briunelli et al.(1988),Narcisi et al.(1972),Kopp(1997)], particularly its inhomogeneities, which were obtained using the method of radio scintillations of a point radio source located on the spacecraft [Briunelli et al.(1988), Gershman et al.(1984), Mityakov et al.(1989)]. The movement of satellites in orbit around the Earth occurs not only under the influence of gravitational forces, but also under the influence of atmospheric drag. Taking into account the drag force of the atmosphere presents problems not only of a mathematical nature, but also of a physical nature. All currently existing models of the Earth's atmosphere (thermosphere) are empirical in nature and depend on factors that have significant stochastic (unpredictable) features. Therefore, fluctuations in atmospheric density cannot be accurately predicted. These difficulties impose serious restrictions on the accuracy of the models and on the time interval over which they can be used [Aksenov(1977)]. By observing the movement of artificial satellites, estimates of the density of the atmosphere at altitudes of 200–300 km and above were obtained [Lidov(1958),Elyasberg(1958), Elyasberg et al.(1960)]. Research has also been conducted on the effect of changes in atmospheric density on the movement of artificial satellites. From books and articles, it is clear that until the 1970s, when studying the dynamics of spacecraft motion, changes in atmospheric density were often not taken into account [Sarychev(1964), Sarychev(1978), Frik(1970)] or only changes due to the altitude profile of the atmosphere were taken into account [Frik(1970), Beletsky et al.(2000), Beletsky et al.(1984)]. From the available works, it is clear that since the 60s of the last century, it has been known about daily, semi-annual, and other variations in atmospheric density obtained by analyzing changes in the movement of satellites [Cook(1970), Jacchia(1965), Jacchia(1967), Jacchia(1967)]. Based on these and other data on variations in atmospheric density, as well as changes in the temperature of the upper layers of the atmosphere, the upper atmosphere was modeled, and models of the upper atmosphere were compiled. One of these was the American model for predicting the orbit of artificial satellites – general perturbation model (SGP) [Liu Ya-Ying et al.(1995), Jacchia et al.(1963)].

2. Data used

In this work, the B–star drag term (the modified ballistic coefficient) parameter was used, which is part of the TLE (Two Line Elements) data format. This format is produced and supported by NORAD (North American Aerospace Defense Command). The two-line data format dates back to the work of Max Lane in the early 1960s (first published in 1965). The drag effects in Lane's model were described by a spherically symmetric model of the atmosphere, which does not rotate. Co-authored with K. Cranford, in 1969, they published a significantly improved model [Vallado(2006),Lane et al.(1969)]. Lane models were widely used by the military and NASA beginning in the late 1960s. An improved version became NORAD's standard model in the early 1970s, eventually leading to the creation of the TLE format. Continuing their joint work, they developed several models of the perturbed motion of artificial satellites. Among them was the SGP model [Lane et al.(1979)]. The report, Spacetrack No. 3, which was eventually released and includes the complete FORTRAN source code for the SGP4 model. This has led to widespread adoption of this model and data format [Hoots et al.(1980)]. Subsequently, the resulting models were refined and modified by introducing amendments. With the development of computing power, the High Accuracy Satellite Drag Model (HASDM) project appeared in 2005. It was designed to smoothly replace the general disturbance model with a special disturbance model, which would use the internal parametric correction of the Jacchia-70 thermospheric model. Thus, users have data sets on the dynamic changes in atmospheric density at various altitudes almost since the 1960s. In addition, the TLE parameter set was used to obtain actual atmospheric densities [Keating et al.(2000), Picone et al.(2005), Doerksen et al.(2019)].

$$B = \frac{C_D * A}{m}$$

where B – the ballistic coefficient, C_D – the aerodynamic drag coefficient. If the mean free path of air molecules is much larger than the geometric size of the satellite, then C_D is close to 2, A – the midsection area (cross–sectional area of the satellite), m – the satellite mass.

The B–star drag term coefficient is related to the ballistic coefficient by the formula:

$$B^* = B * \frac{\rho_0}{2}$$

where B^* – the modified ballistic coefficient or B–star drag term, B – the ballistic coefficient, ρ_0 – some standard density value for a given altitude. The B–star drag term coefficient has the dimension of $1/R_E$, where R_E=6 371 km is the radius of the Earth.

A number of difficulties arise, some of which are associated with the calculation of the atmospheric wind speed perpendicular to the cross-sectional area of the satellite, and the impossibility of accurately taking into account the C_D parameter. Thus, all models, when estimating the B parameter, correct it so that the calculated parameters correspond to the observed positions of the object in the best way. For this reason, this work uses just this coefficient. The coefficient reflects only the atmospheric effect on the object under study.

The B-star index and data on extreme events of class X were used in recent works. It is shown that there is no obvious dependence between such events, either on the class of the event or on the increase in ultraviolet flux, or on the coordinates of their occurrence. The correlation is better with geomagnetic indices (Bz component) and the interplanetary geomagnetic field [Deleflie et al.(2019)]. Recent work from 2022 also looked for correlations between the drag coefficient of satellites and their physical parameters. It was carried out on the topic of removing space debris from low and medium orbits [Houman et al.(2022)]. Deep machine learning technologies are used to obtain data on the dependence of processes that may be influenced by space weather indices, by simulating equatorial density anomalies and geomagnetic storms. Observations from the CHAllenging Minisatellite Payload satellite are used to train the deep learning network [Wenbo et al.(2023)].

The B–star drag term for the three satellites was taken for the calculation:
1) NORAD ID 04922 - COSMOS 394 with orbit elements: i = 65.8 °; e = 0.0027; r_{min} = 490 km; r_{max} = 517 km.
2) NORAD ID 00063 - TIROS 2 with orbit elements: i = 48.5 °; e = 0.0027; r_{min} = 465 km; r_{max} = 481 km.
3) NORAD ID 00746 - ELEKTRON 1 with orbit elements: i = 60.8 °; e = 0.31; r_{min} = 399 km; r_{max} = 6409 km.
where i – the inclination of the orbit, e – the value of the eccentricity of the orbit, r_{min} and r_{max} – the average value of the minimum and maximum distances from the Earth's surface.

Many factors of gravitational and non–gravitational nature affect the flight of artificial objects in near-Earth orbit. In this work, the factors associated with the gravitational nature are excluded by choosing the B–star coefficient as the analyzed parameter. Solar and geomagnetic activity have a significant impact on the change in the satellite's orbit among the disturbing factors of a non–gravitational nature.

A wide range of indices reflecting the state of space weather is used in this work: W – Wolf numbers; S_p – the total area of the sunspots, F10.7 – the radio emission from the Sun at the wavelength of 10.7 cm, TSI (total solar irradiance) – the solar constant, L_α – the Lyman alpha radiation, TCI – Thermosphere Climate Index, E – the fluxes of electrons with energies greater than 0.6 MeV and 2 MeV, the solar wind parameters, IMF – the interplanetary magnetic field, A_p – the planetary geomagnetic index, D_{st} (Disturbance Storm Time Index) – the index of the intensity of geomagnetic storms.

The Wolf number and the total area of the sunspots characterize the 11–year cycle of solar activity.

The F10.7, TSI, and L_α indices characterize the wave component of solar ionizing radiation.

The radio emission from the Sun at a wavelength of 10.7 cm (F10.7) characterizes the wave flux and correlates with the Sun's ultraviolet and X-ray fluxes.

The TSI is a measure of the amount of solar energy received by a body located at a certain distance from the Sun. For the Earth, TSI is defined as the solar energy received per unit area in the upper atmosphere with an average distance from the Earth to the Sun equal to 1 AU. The TSI is approximately 1.35 kW/m^2. This "constant" changes every day, as does sunspot activity, and over longer periods of time, depending on the solar cycle. This constant reflects the change in the total energy flux of solar radiation.

The Lyman alpha radiation, L_α, is a spectral series in the spectrum of the hydrogen atom, named after the physicist Theodore Lyman, who discovered this series in 1906. The series is formed during transitions of electrons from the high energy levels to the first level in the emission spectrum and from the first level to all others during absorption. L_α is located in the ultraviolet region of the spectrum.

TCI is the "Thermosphere Climate Index", a number NASA publishes every day to keep track of the temperature at the top of Earth's atmosphere–a layer of gas researchers call "the thermosphere". TCI is a number expressed in Watts that tells how much heat nitrogen oxide (NO) molecules in the thermosphere are dumping into space. TCI is based on measurements from the SABER instrument onboard NASA's TIMED satellite. SABER monitors infrared emissions from carbon dioxide (CO_2) and nitric oxide (NO), two substances that play a key role in the energy balance of air 100 to 300 kilometers above our planet's surface. By measuring the infrared glow of these molecules, SABER can assess the thermal state of gas up there.

The electron fluxes with energies greater than 0.6 MeV and 2 MeV, and the solar wind parameters reflect the corpuscular component of the solar activity. They influence ionospheric currents and magnetospheric dynamics .

The indices IMF, A_p, and D_{st} show the disturbance of the interplanetary environment, the magnetosphere's reaction to changes in the conditions in the interplanetary environment, and the intensity of disturbances in the magnetosphere, respectively.

The interplanetary magnetic field, IMF, is a component of the solar magnetic field, which is pulled from the solar corona by the flow of the solar wind and fills the solar system.

The planetary geomagnetic index, A_p, characterizes the degree of the solar activity effect on the magnetosphere.

To analyze the magnetic storms, the D_{st} index is used. It is an axisymmetric component of the perturbed magnetic field with respect to the geomagnetic dipole and is determined on the basis of magnetic field measurements at four near-equatorial stations: San Juan, Hermanus, Kakioka, and Honolulu. The studied time period covers the declining phase of the 23rd solar cycle, the period of a prolonged minimum at the end of the 23rd solar cycle, the ascending, maximum, and declining phases of cycle 24 (03.04.2005–12.09.2017).

3. Data processing

Before working with the data, interpolation was performed using the cubic B-spline method (for time series with gaps), and the data were then normalized to the range 0 to 1. To quantitatively characterize the combined influence of the known factors on the parameter under study, multiple correlation analysis was used. In other words, this analysis is used because the system in which the satellite moves is not closed, and changes in its motion parameters result from the influence of many factors. For multiple correlation analysis, regression procedures are used. To build such a dependence model, it is necessary to take into account some conditions: –In order for the model to correctly reflect the change in the parameter under study, it is necessary to exclude mutually correlated parameters from it; – If possible, include in the model the complete set of factors influencing the parameter under study, taking into account, of course, the first condition. For these two reasons, the first consideration was the cross–correlations between solar and geomagnetic activity indices. The parameter under study in this work is the drag coefficient B–star drag term, which will be referred to as the dependent parameter. The factors influencing it will be called independent parameters; among these factors are the indices of solar and geomagnetic activity mentioned above. Correlation coefficients were constructed with the p-level significance assessment. In the case of correlations, the p-value indicates how much a change in one variable depends on a change in another. The higher the p-value (e.g., 0.05, 5%), the more likely the variables are to be independent of each other. p-level = 0.05 is read as follows: only 5% of the values of the selected variable or variables are random, 95% of the values do not change randomly (Table 1 and Table 2 in supplementary material).

After obtaining the correlation coefficients, I included mutually correlating indices in different regression models (Table 3 in supplementary material) and, after recalculating them, paid attention to four values: the Fisher criterion (F), the p-level assessment (p-level), the multiple correlation coefficient (R^2), and the adjusted multiple correlation coefficient (R^2) (Table 4 in supplementary material). The considered multiple correlation coefficients use residual dispersion, which has the systematic error towards underestimation, the more significant, the more parameters that are determined in the regression equation for the given volume n. That is, the more parameters at x, the closer the residual dispersion to zero and the closer the correlation coefficient will approach 1 even with a weak connection between the dependent parameter and the independent ones. To avoid possible exaggeration of the closeness of the relationship, the adjusted coefficient of multiple correlation is used.

Table 3 shows multiple correlation models for three satellites (see supplementary material Table 3). The set of indices selected for these satellites gives the highest adjusted correlation coefficient for the model. B0 and B are coefficients in the multiple correlation model equations. Empty cells indicate that the given index was not considered in the model for the reasons listed above.

Thus, no matter how hard one tries to include indices, a model that depended on several indices was the result.

In short, the adjusted coefficient of determination excludes the residual dispersion error, which has a systematic error towards underestimation and increases as more parameters are determined in the regression equation for the given volume of n. At the same time, even with a weak connection of factors, the correlation coefficient can approach 1. To assess the possible exaggeration of the closeness of the relationship, the adjusted index (coefficient) of multiple correlation is calculated (Table 4 in supplementary material). In this case, regression models were used to identify the indices that most strongly influence the parameter of satellite drag under study. These indices were then used in cross-spectrum calculations. The cross-spectrum shows how the components of two signals at different frequencies are related to each other (two signals may have frequency components that are correlated and frequency components that are uncorrelated, so the cross-spectrum allows one to identify the relationship between the components of complex signals consisting of many oscillations with different periods, amplitudes, and phases). It is a complex function, so it contains both amplitude and phase information. It can be written as:

$$S_{xy}(f) = X(f) * Y^{*}(f)$$

where: S_{xy}(f) – cross-spectrum at frequency f, X(f) – complex Fourier transform of signal x(t) at frequency f, Y^{*} (f) – complex-conjugate Fourier transform of signal y(t) at frequency f.

The mean absolute deviation (MAD) method in sigma equivalent was used as a reliability assessment measure. It was calculated for cospectral density, cross-amplitude, and gains. It was not used for squared coherence and phase spectrum data, as all quantities vary within a narrow range and with high frequency, leading to erroneous estimates. Therefore, the periods presented in the corresponding subchapters were subsequently written taking into account the obtained periodicities for the cross-amplitude data. For real and imaginary parts of the cross-spectrum, it was not calculated, as the graphs were needed for a qualitative assessment of the periods already obtained in the previous subchapters.

4. Results

For the analysis, I selected the following characteristics of the dependence of two time series, which can be obtained using cross-spectral analysis: cospectral density, cross-amplitude, squared coherency, gains, phase spectrum, and real and imaginary parts of cross-spectrum.

4.1. Cospectral density

The cospectral density is computed by smoothing the real part of the cross-periodogram or cross-spectrum. It shows the correlation between signals at different frequencies. It is a way of showing at what frequency two other signals are "in sync" or related to each other (Fig.1). Figure 1 shows an example of a cospectral density graph for the index, which I take as the primary parameter influencing satellite drag in the upper layers of the atmosphere (see Table 3 in supplementary material). If the cospectral density is positive, it indicates a positive correlation between two time series at a certain period. If it is negative, it indicates a negative correlation. If it is zero, there is no connection between the time series.

The main periods obtained from the cospectral density plots are presented in Table 5 (see supplementary material).

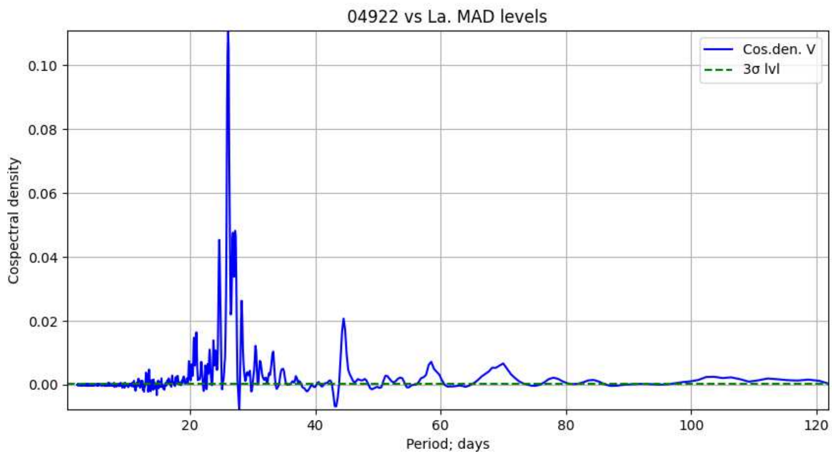

Fig. 1. Cospectral Density between index L_α and B-star drag term for satellite 04922 without trend component for all observation period

4.2. Cross–amplitude

Cross–amplitude shows the strength of the relationship between two signals at each frequency (the correlation between the quasi-periodic components hidden in the signals, a kind of analogue of covariance, but in the frequency domain). The peak in the cross-amplitude spectrum shows that the two compared time series contain hidden quasi-sinusoidal components of variability that are similar in shape and amplitude (Fig.2). Figure 2 shows an example of a cross-amplitude graph for the index, which I take as the primary parameter influencing satellite drag in the upper layers of the atmosphere.

The main periods obtained from the cross–amplitude plots are presented in Table 6 (see supplementary material).

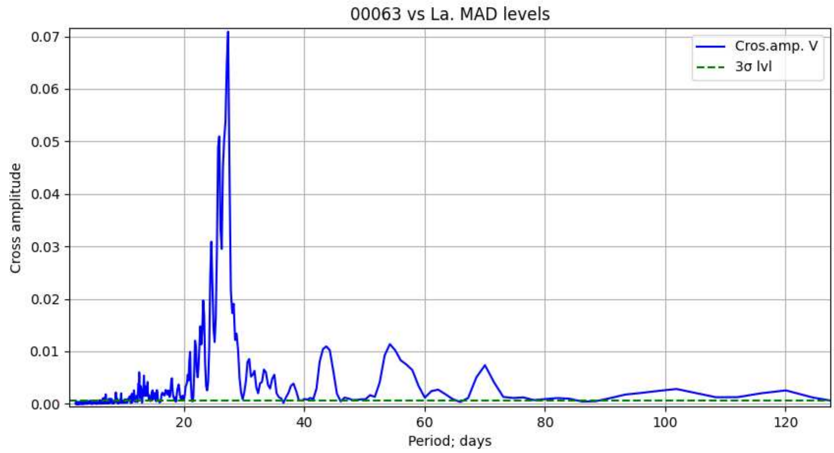

Fig. 2. Cross–amplitude between index L_α and B-star drag term for satellite 00063 without trend component for all observation period

4.3. Squared coherency

Squared coherency shows how linearly related two signals are at each frequency. Values range from 0 to 1, where 1 means a complete linear relationship. The "tail" part of the coherence spectrum is meaningless (only the "signal" part is informative, i.e., the region of the spectrum where the physical periods are), because dividing by small numbers gives large numbers (close to one), which is spurious. Therefore, smoothing of the coherence spectrum is applied by a shift-free moving average, cubic spline, or spectral window (Fig.3). Figure 3 shows an example of a squared coherency graph for the index, which is taken as the primary parameter influencing the drag of satellites in the upper layers of the atmosphere.

The main periods obtained from the squared coherency plots are presented in Table 7 (see supplementary material).

4.4. Transfer function magnitude

Transfer function magnitude (gains): gain spectra show how much one signal is amplified relative to another at each frequency (Fig.4). Figure 4 shows an example of a gain spectrum graph between the index Dst and the B-star drag term. Significant fluctuations in the density and speed of the solar wind will lead to the generation of magnetospheric plasma waves with periods that are multiples of the main periods of the density and speed of the solar wind, which are the cause of the generation of geomagnetic pulsations as an observable manifestation of plasma waves on Earth and in the Earth's magnetosphere.

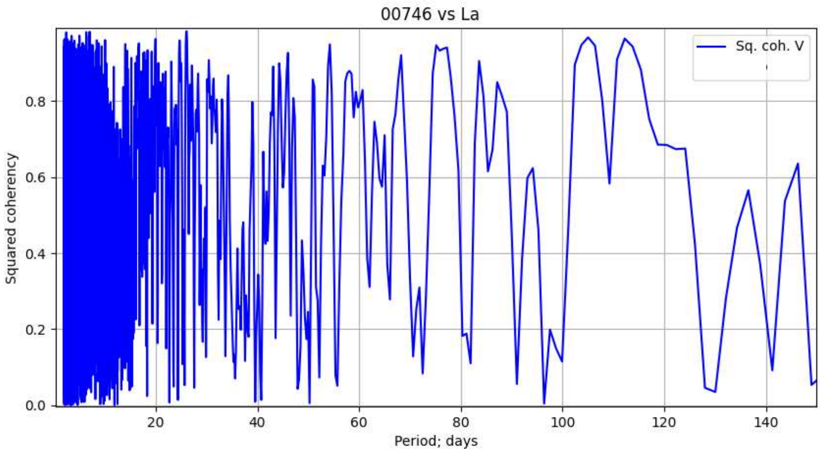

Fig. 3. Squared coherency between index L_α and B-star drag term for satellite 00746 without trend component for all observation period

The main periods obtained from the gains plots are presented in Table 8 (see supplementary material).

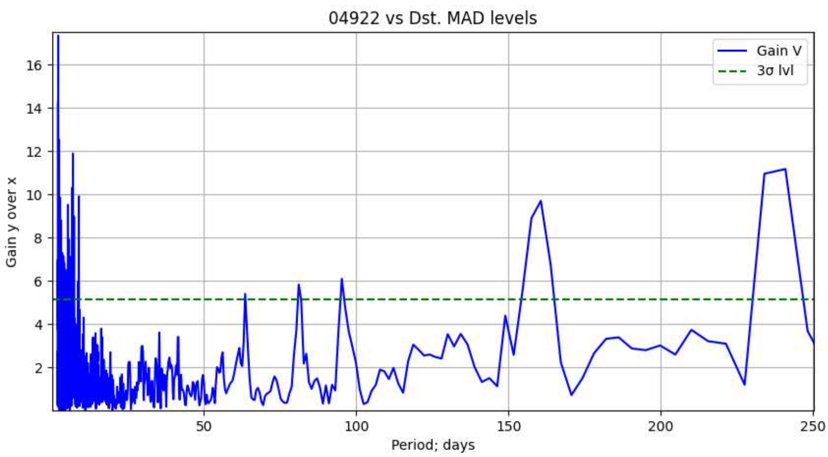

Fig. 4. Gain spectra between index D_{st} and B-star drag term for satellite 04922 without trend component for all observation period

4.5. Phase spectrum

The phase spectrum shows the phase shift between the signals at each frequency. The greater the range of oscillations on the graph, that is, when the graph reaches or is close to the range of $-180°$ to $180°$, this means that in this part of the phase spectrum, there is no relationship between the signals; they are out of phase. On the contrary, the more the phase spectrum has a smooth form of rise, fall, or linear type, the more the signals are connected in the frequency range (periods); these are areas of phased variations in the studied time series. A positive cross-phase means that the signal x(t) is ahead of the signal y(t) at a given frequency, while a negative cross-phase means that it is behind (Fig.5). Figure 5 shows an example of the phase spectrum graph between the index Electron flux>2 MeV and the B-star drag term. When electron fluxes reach the upper atmosphere, they ionize atoms and molecules and release energy that heats the thermosphere. This heating causes thermal expansion of the atmosphere, which results in an increase in density at certain altitudes (especially at 300–600 km).

The main periods obtained from the phase spectrum plots are presented in Table 9 (see supplementary material).

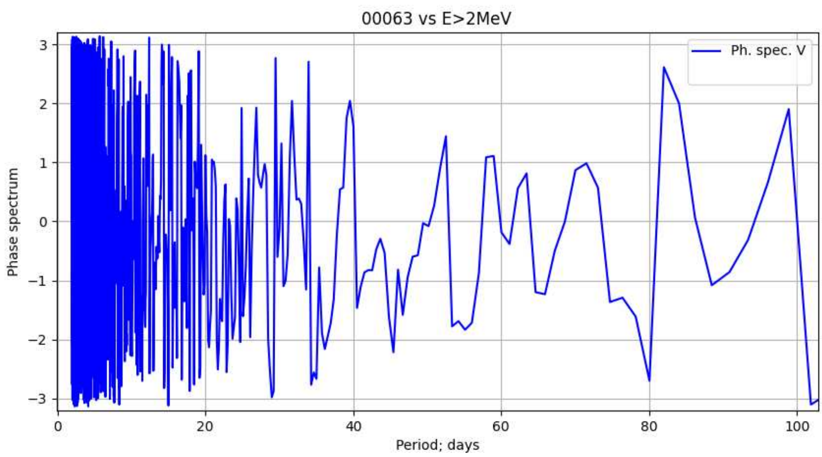

Fig. 5. The phase spectrum between index E>2MeV and B-star drag term for satellite 00063 without trend component for all observation period

4.6. Real and Imaginary parts of cross-spectrum

The real part of the cross-spectrum shows how strongly the signals x(t) and y(t) are correlated at frequency f when in phase, that is, when their phases coincide. In other words, it reflects the components of the signals that oscillate in phase with each other at a given frequency. It represents the "in-phase" component of the cross-spectrum, in contrast to the imaginary part, which represents the "quadrature" component (phase shift by 90 degrees). If the real part is large, it indicates that the two signals have a strong correlation relationship at that frequency without a significant phase shift. The imaginary part shows the correlation of signals with a phase shift of 90 degrees. High values of the imaginary part indicate the presence of a phase shift between the two signals at a certain frequency. Figure 6 shows an example of real and imaginary parts of the cross-spectrum between the index Flow pressure and the B-star drag term for satellite 00746.

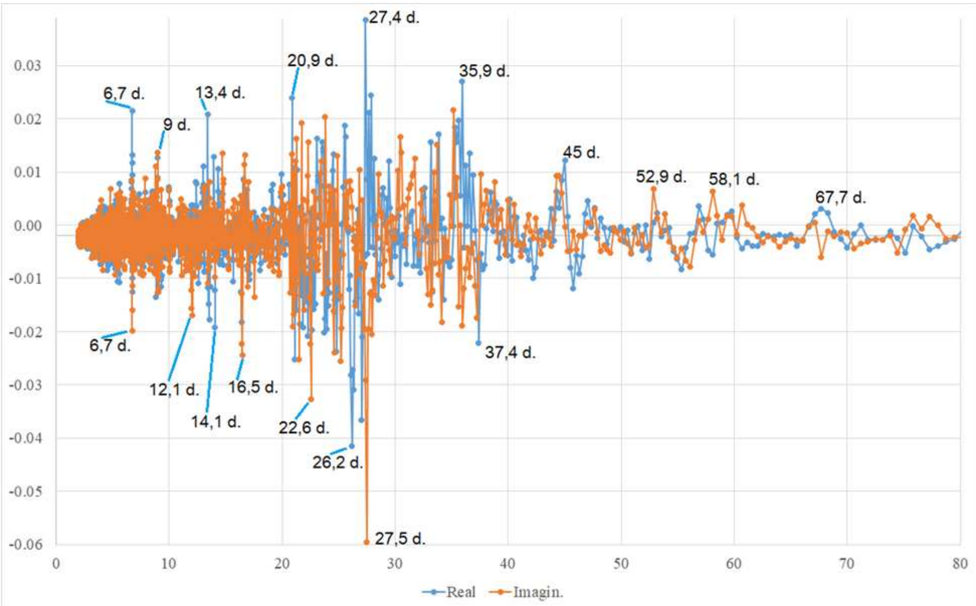

Fig. 6. The real and imaginary parts of cross-spectrum between index Flow pressure and B-star drag term for satellite 00746 without trend component for all observation period (x axis in days)

In other words, if the real and imaginary parts at the obtained frequency (period) are both positive, this means that the two time series have a stable phase relationship at this period. In this case, they oscillate together and one of the time series is slightly ahead of the other. If the real part is positive and the imaginary part is negative, this means that there is a relationship between the periods of these time series, but one of the time series lags behind the other at this frequency/period. If the real part is negative, then there is no dependence between the two time series at a given frequency (period). The graphs of the real and imaginary parts, for all three objects and the selected indices of solar and geomagnetic activity, showed that most of the found common periodicities are in a stable phase relationship (the first case described in the previous paragraph). There are also periods in which there is a delay in the reaction of the drag coefficient, but in smaller quantities.

The most noticeable periods in which there is a delay in the reaction of the drag coefficient from the real and imaginary parts of cross-spectrum plots are presented in Table 10 (see supplementary material).

5. Conclusions

From the cospectral density graphs, a set of in-phase periods for the satellite's drag coefficient, and the selected indices of solar and geomagnetic activity were obtained. Based on the MAD for the selected time series, all the obtained periodicities are above the 3σ confidence level.

The obtained periods reflect the cyclicity of solar activity, with rotation periods of 25-27 days and 30-40 days for the equatorial, mid-latitude, and polar regions of the Sun. These also correspond to the rotation periods of coronal holes, which are the source of high-speed particle flows. On some cross-amplitude graphs, the 13-day period is dominant for indices characterizing the parameters of the solar wind or electron flows. Shorter periods from 6 to 9 days have the greatest amplitude on the graphs of the relationship between B-star and: D_{st}, E>0.6 MeV, E>2 MeV, Solar wind parameters. Perhaps these parameters also affect the emergence of these periods via the ring current, whose intensity depends on the solar wind and the interplanetary magnetic field.

The squared coherency graphs show that the relationship between the satellite's drag coefficient and the selected indices is linear at almost all frequencies. For electron flows, these graphs show a nonlinear relationship, but there are still coherence values above 0.8.

The transfer function magnitude plots (Gains) show that the selected parameters of the solar wind, electron fluxes and D_{st} affect the gain of periodicities from 5 to 10 days, and the main parameter L_α has a stronger effect on the gain of long-period variations from 20 days and more, which agrees well with the results presented above. For all three objects, the 13-day (13,5-13,8 d) period shows a significant increase in the plots of the L_α index. This period represents half of the 27-day cycle and reflects the influence of active regions and solar processes located near the limb of the solar disk [Donnelly et al.(1986), Kane et al.(1995), Salakhutdinova(1999), Tobiska et al.(1989)].

The phase spectrum graphs are quite difficult to analyze because they have very noisy "tails" at short periods. This is because the data in this work represent discrete time series (limited in time) of continuous processes with equal time steps. They are formed by processes that contain changes that are difficult to predict (only with a certain accuracy and over short time intervals) or cannot be predicted at all (random changes). All this imposes certain limitations on the digital processing of these data with methods based on the Fourier transform. Even though methods for suppressing noise instability have been developed, they do not completely remove noise. To construct phase spectrum plots, the complex spectra of the original data series are used. Therefore, if at high frequencies the power of noise processes is close to or exceeds the power of the actual signals (low signal-to-noise ratio), this will lead to a strong scattering of the phase spectrum (i.e., instability of the frequency and phase of the period, or, in other words, random variations). At low frequencies, where the main strong periodicities that contribute most to the data variations are located, the effect of noise components will not lead to instability of the frequency and phase of these periodicities (at least not to a significant extent). Therefore, phase spectrum plots are analyzed together with other estimates obtained from cross-spectral analysis. For the detection of high-frequency periodicities, this means the appearance of false periods with unstable phases, which are statistical artifacts rather than actually existing periodicities. The MAD significance assessment method is not suitable for phase spectrum plots and squared coherence plots, which was written about at the end of Chapter 3. For the L_α index, a distinct phase relationship is visible on periods of 25-30 days and more, and its oscillations are ahead of the B-star oscillations, which is logical. For the two objects 04922 and 00746, the phase relationship is similar based on the graphs. However, for object 00063, electron fluxes >2 MeV show a visible phase relationship with B-star on periods of 40 to 70 days and 20 days. For the geomagnetic storm index, the dependence is not visible in the phase spectrum graph (also for 04922 and 00746).

From the graphs of the real and imaginary parts of the cross-spectrum, it can be seen that for all objects, at the obtained periodicities, there are stable phase relationships. The periods during which the response of the drag coefficient is delayed are recorded in the subchapter 4.6.

Supplementary material

Acknowledgments:
A. Sukharev was supported by Postdoctoral research grant: "Research on Space Weather During Solar Cycle 25 Observed Along the "Struve Geodetic Arc", No. 1.1.1.9/LZP/1/24/048 is implemented in Ventspils University of Applied Sciences and is co-financed by the European Regional Development Fund.

References

Aksenov E. P., 1977, *Theory of Motion of Artificial Earth Satellites. Moscow: Nauka, 360 p.*
Beletsky V. V., Yanshin A. M., 1984, *Influence of Aerodynamic Forces on the Rotational Motion of Artificial Satellites. Kyiv: Naukova Dumka, 188 p.*
Beletsky V. V., Pivovarov M. L., 2000, *On the Influence of the Atmosphere on the Relative Motion of a Dumbbell-Shaped Satellite. Applied Mathematics and Mechanics, Vol. 64, № 5, p. 721–731.*
Briunelli B.E., Namgaladze A.A.,1988, *Ionospheric physics. M.: Nauka, 528 p.*
Cook G.E., 1970, *The semi-annual variation in the upper atmosphere during 1967 and 1968 // Planetary and Space Science, Vol. 18, Issue 11, p. 1573-1584.*

Deleflie F., Briand C., Doerksen K., Sammuneh M.A., Sagnières L., 2019, *Atmospheric Density Variations and Orbit Perturbations in Relation to Isolated Solar X-flare Events // EGU General Assembly Conference Abstracts, EGU General Assembly Conference Abstracts, p. 15338*

Doerksen K., Sagnières L., Deleflie F., Briand C., Sammuneh M. A., 2019, *A Statistical Analysis of Density Perturbations in Relation to Solar X-Flare Events Isolated from Coronal Mass Ejections. // 99th Annual AMS Meeting 2019, held in Phoenix, AZ, 6-10 January 2019, Session: 16th Conference on Space Weather / Space Weather Posters, id. 206. Bibcode: 2019AMS....9953282D*

Donnelly R. F. , Hinteregger H. E. , Heath D. F., 1986, *Temporal variations of solar EUV, UV, and 10,830-Å radiations // Journal of Geophysical Research. Volume 91, Issue A5, p. 5567-5578, DOI: 10.1029/JA091iA05p05567.*

Elyasberg P. E., 1958, *Determination of the Upper Atmosphere Density from Secular Variations of Orbital Elements of the First Two Artificial Earth Satellites. Artificial Earth Satellites, Moscow: Publishing House of the USSR Academy of Sciences, № 1, p. 21–24.*

Elyasberg P. E., Yastrebov V. D., 1960, *Determination of the Upper Atmosphere Density from Observations of the Third Artificial Satellite of the Earth. Artificial Earth Satellites, Moscow: Publishing House of the USSR Academy of Sciences, № 4, p. 18–30*

Frik M. A., 1970, *Stability of Satellite Orientation Under Gravitational and Aerodynamic Torques. Rocket Technology and Astronautics, Issue 10, p. 54–61.*

Gershman B. N., Yerukhimov L. M., Yashin Y. Y., 1984, *Wave Phenomena in Space Plasma. Moscow: Nauka, 392 p.*

Hoots Felix, Roehrich Ronald, 1980, *Models for Propagation of NORAD Element Sets.*

Houman Hakima, Michael C.F. Bazzocchi, Benjamin Almstrom, 2022, *Analysis of Satellite Drag Coefficients Based on Physical and Orbital Specifications. IEEE Aerospace Conference (AERO), ISSN: 1095-323X, DOI: 10.1109/AERO53065.2022.9843417*

Jacchia L. G.; Slowey J., 1963, *Atmospheric Heating in the Auroral Zones: a Preliminary Analysis of the Atmospheric Drag of the Injun III Satellite // SAO Special Report, №136.*

Jacchia L. G., 1965, *Density Variations in the Heterosphere. SAO Special Report, №184.*

Jacchia L. G., 1967, *Recent Results in the Atmospheric Region above 200 km and Comparisons with CIRA 1965. SAO Special Report, №245.*

Jacchia L. G., 1967, *Properties of the Upper Atmosphere Determined from Satellite Orbits. Philosophical Transactions of the Royal Society of London. Series A, Mathematical and Physical Sciences,Vol. 262, № 1124, p. 157-171.*

Kane R. P. , de Paula E. R. , Trivedi N. B., 1995, *Variations of solar EUV, UV and ionospheric foF2 related to the solar rotation period // Annales Geophysicae. Vol. 13, Issue 7, p.717-723, DOI: 10.1007/s00585-995-0717-4.*

Keating G. M., Tolson R. H., Bradford M. S., 2000, *Evidence of long term global decline in the Earth's thermospheric densities apparently related to anthropogenic effects // Geophys. Res. Lett., 27(10), 1523– 1526.*

Kopp E.,1997, *On the abundance of metal ions in the lower ionosphere. JRL, Vol. 102, p. 9967–9974.*

Lane Max, Cranford Kenneth, 1969, *An improved analytical drag theory for the artificial satellite problem // AIAA paper, № 69-925.*

Lane Max, Hoots Felix, 1979, *General Perturbations Theories Derived from the 1965 Lane Drag Theory.*

Lidov M. L., 1958, *Determination of Atmospheric Density from the Observed Drag of the First Artificial Earth Satellites. Artificial Earth Satellites, Moscow: Publishing House of the USSR Academy of Sciences, № 1, p. 9–20.*

Liu Ya-Ying, Chen Zhao, 1995, *An analysis of the influence of various atmospheric models on the drift and life time of a space station // Acta Astronautica, Vol. 35, Issues 2–3, p. 99-105.*

Mityakov N. A., Grach S. M., Mityakov S. N., 1989, *Results of Science and Technology. Series: "Geomagnetism and the Upper Atmosphere," Vol. 9. Ionospheric Disturbances by High-Power Radio Waves. Moscow: VINITI, 138 p.*

Narcisi R.S., Bailey A.D., Wlodyka L.E., Philbrick C.R.,1972, *Ion composition measurements in the lower ionosphere during the November 1966 and March 1970 solar eclipse. JASTP, Vol. 34, p. 647–658.*

Picone J. M., Emmert J. T., Lean J. L., 2005, *Thermospheric densities derived from spacecraft orbits: Accurate processing of two-line element sets // JOURNAL OF GEOPHYSICAL RESEARCH, VOL. 110, A03301, doi:10.1029/2004JA010585.*

Salakhutdinova I. I., 1999, *Identifying the quasi-regular and stochastic components of solar cyclicity and their properties // Solar Physics. Vol. 188, Issue 2, p. 377-396, DOI: 10.1023/A:1005265229175.*
Sarychev V. A., 1964, *Effect of Atmospheric Drag on the Gravitational Stabilization System of Artificial Earth Satellites. Cosmic Research, Vol. 2, № 1, p. 23–32.*
Sarychev V. A., 1978, *Exploration of Outer Space. Vol. 2. Problems of Orientation of Artificial Satellites. Moscow, 223 p.*
Tobiska W. Kent , Bouwer S. David, 1989,*Intermediate-term variations of chromospheric and coronal solar flux during high solar cycle 21 activity // Geophysical Research Letters. Volume 16, Issue 8, p. 779-782, DOI: 10.1029/GL016i008p00779.*
Vallado David, Crawford Paul, Hujsak Richard, Kelso Ted, 2006, *Revisiting Spacetrack Report №3.*
Wenbo Li, Libo Liu, Yiding Chen, Zhuowei Xiao, Huijun Le, Ruilong Zhang, 2023, *Improving the Extraction Ability of Thermospheric Mass Density Variations From Observational Data by Deep Learning // AGU (Advancing Earth and Space Sciences) Space Weather. Volume21, Issue7. https://doi.org/10.1029/2022SW003376*